4-17-2018

The variability in the morphological active width: Results from physical models of gravel-bed braided rivers

Sarah Peirce

Pauline Leduc

Peter Ashmore
pashmore@uwo.ca

The Variability in the Morphological Active Width: Results from Physical Models of Gravel-Bed Braided Rivers

Journal:	*Earth Surface Processes and Landforms*
Manuscript ID	ESP-17-0470.R1
Wiley - Manuscript type:	Research Article
Date Submitted by the Author:	29-Mar-2018
Complete List of Authors:	Peirce, Sarah; The University of Western Ontario, Geography Ashmore, Peter; University of Western Ontario, Geography Leduc, Pauline; Western University, Department of Geography
Keywords:	active width, braided river, bedload, river morphology, photogrammetry

The Variability in the Morphological Active Width: Results from Physical Models of Gravel-Bed Braided Rivers

Sarah Peirce[1*], Peter Ashmore[1], Pauline Leduc[1]

[1] The University of Western Ontario, London, Ontario, Canada

Corresponding Author: Sarah Peirce (speirce@uwo.ca)

Short Title:

Morphological Active Width: Physical Models of Braided Rivers

Key Points

- The morphological active width is a fundamental parameter of braided rivers that increases with total and dimensionless stream power.
- The morphological active width has a positive relationship with bulk change, bedload transport, and active braiding intensity.
- Both morphological change and bedload transport rates were largely undetectable under a dimensionless stream power of ~0.09.

Abstract

The morphological active width, defined as the lateral extent of bed-material displacement over time, is a fundamental parameter in multi-threaded gravel-bed rivers, linking complex channel dynamics to bedload transport. Here, results are presented from 5 constant discharge experiments, and three event hydrographs, covering a range of flow strengths and channel configurations for which morphological change, bedload transport rates, and stream power were measured in a physical model. Changes in channel morphology were determined via differencing of photogrammetrically-derived digital elevation models (DEMs) of the model surface generated at regular intervals over the course of ~115 hours of experimental runs. Independent measures of total bedload output were made using downstream sediment baskets. Results indicate that the morphological active width increases with total and dimensionless stream power and is strongly and positively correlated with bulk change (total volume of bed-material displaced over time) and active braiding intensity (ABI). Although there is considerable scatter due to the inherent variability in braided river morphodynamics, the active width is positively correlated with independent measurements of bedload transport rate. Active width, bulk change, and bedload transport rates were all negligible below a dimensionless stream power threshold value of ~ 0.09, above which all increase with flow strength. Therefore, the active width could be used as a general predictor of bulk change and bedload transport rates, which in turn could be approximated from total and dimensionless stream power or ABI in gravel-bed braided rivers. Furthermore, results highlight the importance of the active width, rather than the morphological active depth, in predicting volumes of change and bedload transport rates. The results contribute to the larger goals of better understanding of braided river morphodynamics, creating large

high-resolution datasets of channel change for model calibration and validation, and developing morphological methods for predicting bedload transport rates in braiding river systems.

Keywords: active width, braided river, bedload, river morphology, photogrammetry

Introduction

Observations in gravel-bed rivers indicate that bedload transport is generally restricted to narrow, often discontinuous, bands of activity along the channel (Davoren and Mosley, 1986; Carson and Griffiths, 1989; Haschenburger and Church, 1998; Lisle et al., 2000; Ferguson, 2003). The lateral extent of these bands, the active width, is spatially and temporally variable, but on average increases with stream power (discharge) in stable, single-threaded channels as well as more complex, braided channels (Haschenburger and Wilcock, 2003; Bertoldi et al., 2009a; Ashmore et al., 2011).

The role of the active width is of particular interest and importance in braided rivers (Bertoldi et al., 2010; Ashmore et al., 2011). Braided rivers accommodate changes in discharge through adjustments in wetted width and braiding intensity (BI) (i.e., number of anabranches), with relatively little change in mean depth and bed shear stress (Ashmore and Sauks, 2006; Bertoldi et al., 2010; Williams et al., 2015; Redolfi et al., 2016). As a result, bedload transport in braided rivers is more responsive to changes in wetted width and active width than to changes in depth and mean bed shear stress, which are the primary controls on bedload flux in single-thread channels (Bertoldi et al., 2009a). Although data are limited, current estimates indicate that the active width of

braiding channels is rarely greater than 50% of the wetted width under channel-forming conditions and, depending on relative bed particle mobility, may be as little as 10% (Mosley, 1987; Bertoldi et al., 2010; Ashmore et al., 2011). There is also evidence that larger active width ratios (active width/ total wetted width) are associated with larger active braiding intensity (ABI, i.e., number of anabranches transporting bedload) (Bertoldi et al., 2009b; Ashmore et al., 2011) but even so, many braiding gravel-bed rivers are restricted to relatively few (often less than 3) active channels at a given time (Mosley, 1987; Egozi and Ashmore, 2009). This follows from observations in the field and laboratory that indicate that a large proportion of the channel flow (up to 95%) can be conveyed by a single anabranch (Mosley, 1982; Egozi and Ashmore, 2009).

The active width is highly variable at a given discharge as a result of the inherent instability of braided river morphology due to changes the convergence and divergence of flow, and the local patterns of erosion and deposition caused by bar formation and migration, as well as channel avulsion (Mosley, 1987; Bertoldi et al., 2010; Ashmore et al., 2011), all of which also contribute to the variability in bedload transport rates (Davies, 1987; Hoey and Sutherland, 1991; Warburton and Davies, 1994; Shvidchenko and Kopaliani, 1998). These complex braiding processes are responsible for reworking large portions of a braided river over a single flood event even when the active width is restricted to a few channels and limited in lateral extent (Mosley, 1982, 1983; Bertoldi et al., 2010).

Given the positive relationship between active width and ABI, and the fundamental association with morphodynamic processes, the active width is expected to be a meaningful parameter for linking complex braided river morphodynamics and the

corresponding bedload transport flux (Bertoldi et al., 2009a; Ashmore et al., 2011; Lugo et al., 2015; Redolfi et al., 2017). Research has already demonstrated that active width, ABI, and bedload transport rates are positively correlated with dimensionless unit stream power (ω*):

$$\omega^* = \frac{QS}{b\sqrt{g\Delta D_{50}^3}} \quad (1)$$

where Q is discharge, S is slope, D_{50} is median grain size, Δ is relative submerged density, b is the average wetted width and g is the acceleration due to gravity, but these relationships have not been systematically investigated (Bertoldi et al., 2009a, 2009b; Ashmore et al., 2011). If robust, these relationships could provide a pathway for predicting bedload transport rates, a notoriously difficult problem in gravel braided rivers, in addition to contributing to understanding the wide variations in transport rate that occur even under constant discharge conditions (Young and Davies, 1990; Ashmore, 1991a; Hoey and Sutherland, 1991). From this, Ashmore et al. (2011) searched for a general relationship for predicting the active width from simple parameters that would be applicable over a range of river conditions (i.e., slope, discharge, and grain size). To do this, the authors measured the active width hydraulically and morphologically. The hydraulic approach was used to compute instantaneous active widths, the lateral extent of grain motion, through simple 1D hydraulic calculations using cross-section surveys in both physical models and full-scale rivers and a standard Shields entrainment threshold. The morphological active width, which represents the lateral extent of bed-material displacement over time, was measured from repeat cross-sectional surveys in the field and from repeat digital

elevation models (DEMs) in a physical model. Bertoldi et al. (2009a) and Ashmore et al. (2011) plotted the dimensionless active width ratio (average active width/ wetted width) against dimensionless stream power (ω^*) and uncovered a strong linear relationship between the dimensionless parameters indicating that the active width is a fundamental property of braided river morphodynamics. Furthermore, as dimensionless stream power can be calculated from relatively little information, this relationship offers a simple method for estimating active width from basic channel geometry and grain size measurements (Bertoldi et al., 2009a; Ashmore et al., 2011). However, these results were based on relatively few empirical measurements and a limited range of dimensionless stream power and have not been consistently or systematically investigated over a range of braided river morphology and discharge, or directly compared to measurements of bedload flux.

Here, we characterize the variability in the morphological active width in gravel-bed braided rivers and analyze its relationship with measurements of bedload transport rates and stream power. Unlike the 'snapshot' of bedload flux defined by the instantaneous active width, the morphological active width only considers the bedload flux responsible for driving the evolution of channel planform and topography (Marti and Bezzola, 2006; Ashmore et al., 2011). Furthermore, while the two definitions of active width are expected to be comparable at sufficiently short-time intervals (Lindsay and Ashmore, 2002), hydraulic predictions of active width are very sensitive to Shields stress and bed material grain size, which are difficult to define for gravel-bed braided rivers (Ashmore et al., 2011). Therefore, the focus here is on the connection between morphological activity and the rate of bedload transport in braided rivers. Given the

need for simultaneous measurements of morphological change and bedload flux, which are practically impossible to obtain in the field (Bertoldi et al., 2010; Redolfi et al., 2017), data was collected from physical models using a combination of digital elevation model (DEM) differencing and downstream sediment baskets. The result is a large novel dataset of morphological change and bedload flux across five formative discharge experiments as well as three simulated event hydrographs, using spatially continuous topographic data taken at high temporal frequency. The use of DEM differencing techniques made it possible to quantify the morphological active width, total volumes of change as well as the morphological active depth (i.e., vertical depth of morphological activity), which has not yet been characterized for braided rivers, but may contribute to overall understanding of river morphodynamics and morphologically-driven bedload transport (Ashmore et al., 2011). By expanding the relatively limited number of morphological active width measurements to date, along with introducing direct measurements of bedload flux, this research has the potential to inform future morphodynamic models, both conceptual and numerical, which cannot currently account for the inherent complexity and morphologically-driven bedload transport of braided rivers (Lugo et al., 2015; Recking et al., 2016; Williams et al., 2016b).

Experimental Set-up

Data was gathered from six Froude-scaled physical models of gravel-bed rivers in a river modelling flume located at The University of Western Ontario (UWO). Froude-scale modelling (FSM) is used in gravel-bed braided river research to preserve geometric and dynamic similarity, and therefore fundamental force ratios, in the model relative to the full-scale river (Ashmore and Parker, 1983; Southard et al., 1984; Ashmore, 1988, 2007;

Young and Davies, 1990; Hoey and Sutherland, 1991). This includes similarity of non-dimensional bed shear stress which is required in FSM for modelling bed particle mobility and related morphodynamic processes (Peakall et al., 1996; Young and Warburton, 1996; Ashmore, 2007; Redolfi et al., 2016). The flume was 18.3 m long and 3 m wide with recirculating water and sediment. Five metal sediment baskets with a mesh size of 0.1 mm were placed in the tail tank across the full width of the model where all sediment output from the flume could be weighed, which allowed for the calculation of a time-integrated bedload transport rate over short time intervals. To maintain similarity in sediment transport and sorting processes between a full scale river and the models, the grain size distribution (GSD) of the flume was scaled down at a ratio of 1:35 from the Sunwapta River, a proglacial braided river located in Alberta, Canada (D_{50} = 41 mm). The result was a model GSD that ranged from 0.18 mm to 16 mm, with a D_{10} of 0.32 mm, D_{50} of 1.18 mm and D_{90} of 3.52 mm. To reduce cohesion and non-similarity of bedforms (e.g., ripples which often form in fine sand regardless of scale), the lower limit of the grain size distribution was truncated so that grains smaller than 0.25 mm were excluded from the bulk flume grain size distribution (Young and Warburton, 1996).

Of the six experiments completed, five were done under constant channel-forming discharge conditions covering a range of total stream power ($\Omega = \rho g Q S$, where ρ is water density, g is gravitational acceleration, Q is discharge, and S is slope) between 0.10 – 0.41 W m^{-1}. Labelled in chronological order, experiments 1, 4, 9, and 12 were completed at 1.5 % slope based on the slope of the prototype river, while experiment 13 was completed at 2 % slope in order to extend the range of total stream power (Figure

1a and Table 1). A sixth experiment, experiment 11, was run in the form of three event hydrographs (A, B, and C) at 1.5% slope (Figure 1b) where the peak model discharge of 2.1 l s^{-1} was chosen to reflect the average peak diurnal discharge of the Sunwapta River (~ 15 m^3 s^{-1}) based on the 1:35 scaling ratio (Figure 1b and Table 1) (Ashmore and Sauks, 2006; Egozi and Ashmore, 2008). This peak model discharge of 2.1 l s^{-1} was also used during the initial 24 hour evolution of experiment 11.

Each experiment began with a straight trapezoidal channel which evolved at a constant channel-forming discharge towards a channel morphology with a stable average braiding intensity (Ashmore, 1988, 1991b; Egozi and Ashmore, 2009; Ashmore et al., 2011). The initial channel dimensions were chosen to accommodate the imposed discharge without causing wide-spread overbank flooding. This initial evolution generally took less time as total stream power increased, with the exception of experiment 1, which developed a stable morphology after only 16 hours (Table 1). Following the initial channel evolution, two ~ 8 hour blocks of experimental runs were completed. The two blocks of runs were separated by a second, shorter period (~ 8 hours) of evolution and planform reconfiguration in order to capture the wide natural variation of morphodynamics. For each experiment, the ~ 16 hours of experimental runs were divided into 15 intervals, with the exception experiment 1. Morphological methods, like those used here, are sensitive to the time interval between surveys, which must be long enough to allow for a detectable amount of morphological change but short enough that major changes in morphology are not compensated, resulting in no net vertical change (Ashmore and Church, 1998; Lindsay and Ashmore, 2002; Ashmore et al., 2011). For this reason, 15 minutes was chosen as the shortest practical time interval to

use in the flume, but was adjusted to 30 minutes for experiment 1, which had very low, almost undetectable, levels of morphological change after 15 minutes. The reported observations include only the 30-minute runs from experiment 1 and the 15-minute runs from the remaining experiments (4, 9, 11, 12, and 13). At the end of each 15 or 30 minute experimental run, the flow in the model was turned off, the surface drained naturally, and the bedload collected in the downstream baskets was weighed and returned to the tail tank for recirculation. Once the surface was completely drained (i.e., no standing water at low points in the channel), convergent digital images of the entire dry bed model surface were taken using 2 Canon T5i cameras located on a movable camera trolley ~3 m above the model surface as part of the dry bed photo survey. In addition to the dry bed photo survey, photos of the wet bed surface were taken in the last minute of each run, covering the downstream half (~10 m) of the model.

Data Processing and DEM Processing

The software package Agisoft PhotoScan 1.0.0.1 was used for photogrammetric processing to convert both the dry and wet bed photo surveys into high-resolution digital elevation models (DEMs) (Kasprak et al., 2015; Morgan et al., 2016). The photo surveys were batch-processed using a custom Python script, which produced an orthophoto and DEM of each flume surface with 1.5 mm pixels, which is similar to the D_{50} of the model (1.18 mm).

A sample of wet bed orthophotos taken from each experiment were used to quantify a reach-averaged braiding intensity (i.e., average number of wetted channels based on 1 m cross-sectional counts) and wetted width (total area of water in channels divided by reach length), which was manually digitized from the orthophotos using ArcMap 10.4

(Egozi and Ashmore, 2008). For the constant discharge experiments, one wet bed orthophoto was digitized for every two hours of experiment runs for a total of 8 measurements of BI and wetted width each. The exception was experiment 1, where only 4 orthophotos were digitized due to the stable BI and essentially constant wetted width. For the hydrograph experiment 11, one orthophoto was digitized for each discharge step for a total of 26 measurements of BI and wetted width.

Examples of final DEMs for each experiment can be seen in Figure 2, where the maximum elevation is between 0.05 – 0.07 m. Experiment 1 maintained a single-threaded morphology with alternate bars throughout the length of the experiment, while the rest of the experiments developed a multi-threaded braiding morphology. As experiment 13 left very little of the flume surface untouched, apart from minor areas near the upstream weir and several small areas by the flume edges, the experiments used in this research represent the practical extremes between the low stream power (experiment 1, 0.10 W m^{-1}) and high stream power (experiment 13, 0.41 W m^{-1}) conditions possible in the flume used.

The DEMs were used to quantify topographic change over time. The standard deviation of the average vertical precision for DEMs from each experiment is given in Table 2. Raw DEMs of Difference (DoD) were generated by subtracting successive DEMs (Williams, 2012; Kasprak et al., 2015). An absolute threshold of 3 standard deviations (σ) of the vertical error was applied to each raw DoD, which assuming a normal distribution corresponds to a 99.7 % confidence interval (Table 2). A binary map was created from each thresholded DoD by identifying cells as above (given a value of 1) or below (given a value of 0) the 3σ detection limit. A circular dilation filter with radius of 15

cells (22.5 mm) was applied to this binary map so that ‘0’ cells within close proximity to ‘1’ were also converted to 1. This revised binary mask was applied to the original raw DoD so that only areas classified by a ‘1’ were included when the final change detection threshold of 1 mm was applied. While simple spatially uniform thresholds are commonly used (Vericat et al., 2017), this dilation method considers the neighbours of pixels with a high probability of ‘real change’ and therefore was chosen to include probable areas of change that would be excluded with a uniform threshold while also eliminating ‘speckling’ from the DoDs. The DoDs used for the final analysis were cropped to exclude coded targets on the inside walls of the flume as well as reduce inlet effects so that only the downstream 14 m of the model were used for further analysis.

The total active area, defined as the total area of the flume that had topographic (i.e., morphological) change, was measured from the DoDs as the sum of all erosion and deposition cells multiplied by the cell size. The reach-averaged morphological active width (AW) was then calculated for each experimental run by dividing the total active area (m^2) by the reach (i.e., 14 m) length:

$$AW = \frac{Active\ area}{Reach\ length} \tag{2}$$

By multiplying the elevations (sum of z values) in the active areas of deposition and active areas of erosion by the cell size it was possible to calculate a volume of deposition (V_d) and erosion (V_e). The summed volumes of deposition represent additions to sediment storage (i.e., aggradation of bars) while the summed volumes of erosion represent all of the sediment moving from storage (i.e., eroding banks or bars) (Wheaton et al., 2013). The total volume of morphological change, the bulk change, was

266 then calculated for each experimental run as the sum of those volumes (Wheaton et al., 267 2013):

$$Bulk\ Change = \sum V_d + \sum V_e \tag{3}$$

268 Finally, reach-averaged estimates of the active depth were calculated by dividing the 269 bulk change by the total active area:

$$Active\ Depth = \frac{Bulk\ change}{Active\ area} \tag{4}$$

270 Results

271 The Morphological Active Width

272 The reach-averaged morphological active width was calculated for each experimental 273 run (i.e., each DoD), for a total of 399 measurements across all six experiments (Table 274 1). Examples of DoDs from the end of each constant discharge experiment are 275 presented in Figure 3**.** Based on a preliminary visual inspection of the DoDs, experiment 276 1 had very little topographic change, even over 30 minutes of experimental run time. In 277 experiment 1, erosion and deposition were restricted to a single main channel, with 278 erosion on the outer banks of the channel and deposition on regularly spaced alternate 279 bars. Experiment 4 and 9 showed increased complexity (i.e., greater braiding and active 280 braiding intensity) compared to experiment 1, with some areas clearly showing at least 281 two main active channels, and contiguous areas of erosion and deposition (Figure 3). 282 Experiments 12 and 13 both had multiple active channels, extensive contiguous areas 283 of erosion and deposition, and overall greater depths of erosion and deposition 284 compared to experiments at lower discharge and total stream power (Figure 3).

Example DoDs from the rising limb of hydrograph B in experiment 11 are shown in Figure 4. While experiment 11 runs were completed on a braiding channel developed during initial evolution, the complex channel morphology including multiple anabranches flowing around mid-channel bars, does not become apparent in the DoDs until discharges exceed 1.14 l s^{-1} (Figure 4). At and below this discharge, the active areas of change were generally patchy, discontinuous, shallow, and small in areal extent. Overall, the DoDs from both the constant discharge experiments and the hydrograph experiments highlight three main trends as total stream power increased: 1) the active area, and therefore the reach-averaged morphological active width, became greater; 2) the active areas became more continuous and contiguous as areas of erosion and deposition expanded, and 3) the maximum depths of the morphological active layer increased (Figure 3 and 4).

Values of the reach-averaged morphological active width had an overall positive relationship with total stream power, but were temporally variable within each of the constant discharge experiments (Figure 5a and b). Active width was very low for experiment 1 (n = 28, $\bar{x}$ = 0.015 m) and increased with each increase in total stream power, although there was considerable overlap between the ranges in active width for experiment 4 (0.05 – 0.33 m, n = 65, $\bar{x}$ = 0.17 m) and experiment 9 (0.10– 0.35 m, n = 67, $\bar{x}$ = 0.20 m) (Figure 5a and b). Experiments 12 and 13 had much higher active widths than the rest of the experiments, with averages of 0.57 m (n = 64) and 0.80 m (n = 66), respectively.

As with the constant discharge experiments, the reach-averaged morphological active widths increased with flow strength during the hydrographs but were variable for any

given total stream power and discharge (Figure 5c). Below 0.17 W m^{-1} (1.14 l s^{-1}) there was very little detectable morphological change ($\bar{x}$ < 0.05 m) (Figure 5c and d). Above 0.17 W m^{-1}, the mean active width, as well as its variability, generally increased with increasing discharge. Compared to the constant discharge experiments, the active widths from the hydrograph covered a similar range as experiments 1, 4, and 9, again highlighting the sensitivity of the active width to total stream power.

The frequency histograms of the morphological active width show that all observations from experiment 1 fell between the narrow range of 0 and 0.05 m (Figure 6). The rest of the experiments had frequency histograms defined by a positive skewness coefficient. Experiments 9 and 13 were defined by similar skewness coefficients (0.469 and 0.477, respectively), while experiment 12 had several high reach-averaged active width values resulting in a larger skew coefficient of 0.648 (Figure 6). With the lowest skewness coefficient (0.364), experiment 4 was the closest of the multi-threaded experiments to a symmetrical distribution. The hydrograph experiment 11 was also positively skewed (skew = 0.523) due to the relative abundance (30%) of low active width values (< 0.1m) from the low discharge runs.

Matching the morphological active width measurements to corresponding average wetted width measurements from the sample of digitized wet bed orthophotos, it was possible to estimate a reach-averaged percent active width (Table 3). For experiment 1, which had a very narrow range of wetted widths due to the single-threaded morphology, the active width only accounted for 4 - 9 % of the average wetted area of the model. Experiment 4 and 9 had similar minimum values for percent active width (7.44 and 7.60 %, respectively), but experiment 4 had a greater average (16.5 vs 11.6 %) and

maximum value (27.3 vs. 17.1 %) than experiment 9. This difference may be related to a primary channel in experiment 9 flowing along the side of the flume for several meters during the second half of the experiment, restricting the lateral development and therefore the active area of the channel. As expected, experiments 12 and 13 had the largest percent active widths, with the active width accounting for up to 50 % of the wetted width in experiment 13 (Table 3). The hydrograph experiment, experiment 11, had the greatest range of values, as would be expected given the large range of discharges, but mean and median values close to those found in experiment 9 (Table 3). Given that experiment 9 and 11 evolved under the same formative slope and discharge conditions, this could reflect a tendency for the peak total stream power or discharge to control the morphological scale at which dominant braiding processes occur (Redolfi et al., 2017).

The Morphological Active Depth

Along with the morphological active width, the DoDs were used to derive reach-averaged morphological active depth. The aim was to determine if the active depth behaved in a similar way as the active width, or if the majority of morphological activity in braided rivers is dominated by changes in the morphological active width (Ashmore et al., 2011). Excluding experiment 1, which had very low values for reach-averaged active depth, the overlap in the range of the box plots in Figure 7a indicate that the mean active depth is not very sensitive to the changes in total stream power between the multi-threaded constant discharge experiments (experiment 4, 9, 12, and 13). In general, the mean active depth increased between experiments 1, 4, and 9 from 0.002 to 0.005 m before declining under the higher total stream power conditions of

354 experiment 12 and 13 ($\bar{x} = 0.004$ m). This is likely the result of more complex
355 morphologies at high total stream power distributing the flow among a larger number of
356 active channels and more extensive bar networks, leading to less deep scouring in any
357 particular location even though total discharge and stream power are greater.

358 During the hydrograph experiments, the reach-averaged morphological active depth
359 increased slightly above total stream power of 0.17 W m^{-1} (1.14 l s^{-1}) before levelling off
360 around 0.27 W m^{-1} (1.86 l s^{-1}) (Figure 7b). Yet, overall range of mean active depth was
361 still small (0.002 – 0.005 m) (Figure 7b).

362 **Connecting Channel Morphodynamics to Bedload Transport**

363 Given that the morphological active width was more sensitive to total stream power and
364 discharge than the morphological active depth for both the constant discharge and
365 hydrograph experiments, three additional analyses were completed to see how active
366 width related to other components of channel dynamics and bedload transport. First,
367 bulk change was determined from the DoDs and compared to the morphological active
368 width to determine if the active width might be used as an indicator of total
369 morphological channel change. Second, direct measurements of bedload transport rate
370 from sediment baskets at the downstream end of the model were used to see how the
371 morphological active width corresponded to independent measures of bedload
372 transport. Finally, results from this study were non-dimensionalized to compare with
373 previous data of morphological active widths in braided rivers, specifically as they
374 related to dimensionless stream power and active braiding intensity.

Volumes of Change

Bulk change, the total volume of erosion and deposition for each DoD, increased with total stream power across the constant discharge experiments (Table 4). Like the morphological active width, bulk change was largely undetectable for the single-threaded experiment 1 ($\bar{x}$ = 0.0006 m^3). Across the multi-threaded constant discharge experiments, the mean bulk change increased steadily with each increase in total stream power towards experiment 13, which had the greatest mean bulk change ($\bar{x}$= 0.047 m^3) (Table 4).

As expected, the bulk change was highly variable across the hydrograph experiments, but overall increased with increasing discharge and total stream power. As with morphological active width, mean bulk change was very low at stream power less than 0.17 W m^{-1} ($\bar{x}$ < 0.001 m^3) and then increased with total stream power to a maximum average value of 0.025 m^3 at the peak stream power of 0.31 W m^{-1} (2.1 l s^{-1}). Focusing on the peak total stream power runs (0.31 W m^{-1}), hydrographs A and C had similar average bulk change ($\bar{x}$ = 0.030 and 0.032 m^3 respectively) while hydrograph B had a lower average ($\bar{x}$ = 0.02 m^3). This result may reflect differences in hydrograph structure as hydrograph B had 8 consecutive peak runs while hydrographs A and C each only had 4. Specifically, the first 4 peak runs for hydrograph B had a very similar mean bulk change ($\bar{x}$ = 0.027 m^3) as hydrograph A and C while the last peak runs had an average bulk change half ($\bar{x}$ = 0.013 m^3) that of the first 4 runs. This variability within a given hydrograph and between hydrographs may highlight the importance of antecedent conditions and morphology in determining volumes of morphological change, and ultimately bedload transport rates.

The reach-averaged morphological active width was plotted against the reach-averaged bulk change (bulk change volume divided by reach length) for all six experiments in Figure 8. The overall relationship is strong across all of the experiments (R^2 = 0.965, RMSE = 0.0002) suggesting that active width is a good predictor of bulk change, under both constant discharge and hydrograph conditions. This strong positive relationship further emphasizes that the majority of the morphological activity in braided rivers is dominated by changes in the morphological active width, with relatively little influence from the morphological active depth.

Bedload Transport Rate

Figure 9a shows box plots for the bedload transport rates measured from the downstream sediment baskets for the constant discharge experiments. Experiment 1 had both the lowest mean and lowest range of values ($\bar{x}$ = 0.71 g s^{-1}, σ = 0.25 g s^{-1}). From there, increasing total stream power resulted in an increase in the mean bedload transport rate as well as the relative variability. The average bedload transport rate for experiment 4 was 2.85 g s^{-1} (σ = 1.73 g s^{-1}), while experiment 9 had an average of 4.48 g s^{-1} (σ = 3.30 g s^{-1}). Experiments 12 and 13 had the highest averages with bedload transport rates of 10.44 gs^{-1} (σ = 5.10 g s^{-1}) and 13.30 gs^{-1} (σ = 5.09 g s^{-1}) respectively (Figure 9a). Following the same trend as the active width and bulk change, the mean bedload transport rate and range increased above a lower threshold of 0.17 W m^{-1} (Q = 1.14 l s^{-1}) and then continued to increase with increasing total stream power and discharge during the hydrograph experiments (Figure 9b). Below 0.17 Wm^{-1}, measured bedload transport rates were negligible ($\bar{x}$ = 0.16 - 0.21 g s^{-1}, σ = 0.10 - 0.13 g s^{-1}).

Bedload transport rate has a strong positive power relationship with reach-averaged morphological active width (R^2= 0.701, RMSE = 3.76) (Figure 10). The hydrograph experiment (experiment 11) covered a very similar range of values as the constant discharge experiments 1, 4, and 9, while experiments 12 and 13 extended beyond this range, as expected based on differences in total stream power (Figure 10). Experiment 1 seems to have a greater bedload transport rate than would be expected for the range of active widths, which is either an artifact of the low detection rates for that experiment (i.e., based on the relatively high error estimate, Table 2), or a difference in the mode of transport such that bedload is less involved in dynamically developing morphology and therefore behaves more like a simple, plane-bed flume (Church 2006; Recking et al., 2016). The correlation of the morphological active width with directly measured bedload transport rate in braided rivers at constant discharge and under varying flow conditions has not previously been demonstrated.

The Dimensionless Morphological Active Width

While previous measurements of the morphological active width are relatively limited, Bertoldi et al. (2009a), Ashmore et al., (2011), and Lugo et al., (2015) showed that the variation of active width with discharge or total stream power may collapse to a general function using dimensionless stream power (ω*) and active width ratio (non-dimensionalized using wetted width). Ashmore et al. (2011) also plotted the active width ratio against measurements of ABI in order to asses this basic relationship and to evaluate whether ABI, which can be predicted from wetted width, may be an indicator of relative active width. Focusing only on measured values (not hydraulic computations), the results from this research were combined with braided river results previously

plotted by Ashmore et al. (2011) (Figure 11). The results from the current study help to fill the large gap in previously measured conditions for gravel-bed braided rivers, which included measurements from both field and flume. In terms of dimensionless stream power, the results found here show a similar positive trend and range of values as those previously found, particularly in terms of results from the Sunwapta River (Figure 11a). The Sunwapta data cover a range of dimensionless stream power from 0.078- 0.088, which appeared to be close to the approximate lower limit of dimensionless stream power for non-zero active width (Ashmore et al., 2011). A similar range of dimensionless stream power (0.079 - 0.11) was found at the lower threshold of morphological change (~0.17 W m^{-1}, ~1.14 l s^{-1}) in the hydrograph experiments, which were loosely based on the diurnal hydrograph of the Sunwapta. Note that in Figure 11a, the single-threaded channel (experiment 1) plots away from the rest of the experiments, with a very high dimensionless stream power ($\bar{x}$ = 0.25), but a low active width ratio ($\bar{x}$ = 0.066) (Figure 11a). This reflects a basic distinction in morphodynamics between single-threaded and braided channels. Looking at the active width ratio and ABI (Figure 11b), the results found here enhance the overall positive trend indicating that morphological complexity (i.e., ABI) may be a helpful indicator for morphological active width and, based on Figure 8 and 10, bulk change and bedload transport rates as well. In both plots, differences between the results of this research and those from previous UWO experiments (Figure 11a and b) are apparent. While the previous experiments used the same flume, slope, and grain size as the current data at a discharge of 2.1 ls^{-1} (similar to our experiment 9) there were differences in data collection and analysis that may contribute to the discrepancies. For example, the previous survey interval was 1 hour

rather than the 15- or 30- minute intervals used here In addition, the DoDs were generated using a uniform change detection threshold of approximately 3mm, rather than the more complex dilation method used in the current study. Finally, the measurement of the water surface, and therefore the wetted width, was different (estimates from cross-section topography versus mapping from orthophotos) which has direct effect on the dimensionless variables.

Discussion

The morphological active width increased positively with total stream power and discharge for both the constant discharge and hydrograph experiments, although it was largely undetectable below a threshold total stream power of 0.17 W m^{-1} (1.14 l s^{-1}). While there are few equivalent field observations for a known discharge or over single events, Ashmore et al. (2011) found that morphological active width in the Sunwapta River was largely undetectable for daily meltwater hydrographs with peak discharge below 11-12 m^3 s^{-1}. Based in the 1:35 scaling relation between the Sunwapta and the model, this corresponds with model discharge ~ 1.5 l s^{-1} (~0.2 W m^{-1}) at 1.5 % slope. This estimated threshold is only slightly higher than the 1.14 l s^{-1} (0.17 W m^{-1}) threshold found in these physical model experiments, although the slight difference can be attributed to differences in methods and morphological change detection for the laboratory photogrammetry versus topographic surveys of cross-sections in the field. Above this lower threshold, the morphological active width increased positively with total stream power in both the field (Bertoldi et al., 2010; Ashmore et al., 2011) and flume.

These findings reflect a tendency for wetted width in braiding rivers to increase in response to increased discharge (Ashmore and Sauks, 2006; Redolfi et al., 2016),

489 leading to the expansion of competent flows and the morphological active width laterally
490 across the braidplain (Bertoldi et al., 2010). Furthermore, across all of the experiments
491 the average percent active width ranged from 6 – 45 %, generally increasing with total
492 stream power. This range of values reflects similar results from the field at the
493 Sunwapta River and Tagliamento River, where the percent active width generally
494 ranged from 10 - 40%, but could reach local maximums of 50 - 60% (Bertoldi et al.,
495 2010; Ashmore et al., 2011). Bertoldi et al.(2010) suggest that this large range in active
496 width values from barely detectable to over half of the channel width reflects changes in
497 the spatial scale at which bedload transport processes occur in braided rivers,
498 expanding from local bar and bank erosion to channel wide bifurcations and avulsions.
499 Additional experiments should investigate if percent active width is a regime property of
500 braiding rivers determined by a formative discharge.

501 Amongst the general trends, the morphological active width demonstrated high spatial
502 and temporal variability as a result of dynamic channel morphology across the multi-
503 threaded channel experiments, both at constant discharge and in response to imposed
504 hydrographs. Ashmore et al. (2011) attribute variability in the morphological active width
505 to the complexity of braided rivers and contingency of morphodynamic events (i.e.,
506 fluctuations in ABI, bar development, and avulsion) which are often episodic even at
507 constant discharge. Furthermore, antecedent conditions in the channel may contribute
508 to additional morphological instability through variations in local bed mobility (Ashmore
509 et al., 2011), which can be easily impacted by local grain size distributions and sediment
510 supply (Dietrich et al., 1989). Yet, even with spatiotemporal variability we were able to

expand on the findings of Ashmore et al. (2011) and confirm that dimensionless stream power and ABI can be used as general predictors of an active width.

Unlike the reach-averaged morphological active width, the reach-averaged morphological active depth was not particularly sensitive to changes in total stream power across the constant discharge experiments, and remained in a relatively narrow range of 0.003-0.007 m for all four multi-threaded experiments (i.e., experiments 4, 9, 12, and 13). Looking to the field, Vericat et al. (2017) also reported that while volumes of erosion and deposition were highly variable in the braided Rees River, depths of change were generally similar between flood events. Comparing the active depth findings with the results of the active width confirm that increases in discharge were largely accommodated by increases in the wetted width, active area (i.e., active width), and active braiding intensity, with relatively little change in active depth. During the hydrograph experiments there was a noticeable increase in active depth with stream power above 0.17 W m^{-1} before leveling off under the highest total stream power conditions (0.31 W m^{-1}). The shift in active depth around 0.17 W m^{-1} could reflect the transition from the below threshold condition to the above the threshold for local grain entrainment.

Given that the morphological active depth did not respond strongly to changes in total stream power, the morphological active width was plotted against bulk change and direct measurements of bedload transport rate and found to have a strong positive relationship in both cases. To our knowledge, these plots have not be generated before, likely due to the challenges of directly, and simultaneously, measuring morphological change and bedload transport rates.

In addition, the results indicate that the morphological active width, bulk change, and bedload transport rates all experience a similar lower threshold for detection around 0.17 W m^{-1} (1.14 l s^{-1}, ω* ~ 0.09) indicating that in dynamic rivers, there is no significant bedload transport without detectable net morphological change at the channel scale. Bedload entrainment thresholds have classically been defined at the grain scale (see Buffington and Montgomery, 1997) but evidence from these experiments indicate that the grain-scale bedload threshold may be the same (or very similar) to the threshold for detectable morphological change in braided rivers. The significance of this finding is that it confirms that bedload transport in braided rivers is not simply grains exchanging on a static bed, but active erosion and deposition that is both driven by, and controlled by, the morphology of the river. This is new and requires assessment with data from other physical models as well as field data which could extend these general relationships to greater dimensionless stream power as well as explore the effect of different hydrograph shapes, flood conditions (i.e., above bankfull), grain size distributions, and sediment supply on the morphological active width. In relation to sediment supply in particular, sediment recirculation imposed approximate input-output balance on the model and it is possible that relationships may differ in situations in which input and output do not balance.

Moving forward, the ability to define a general morphodynamic threshold coupling bedload transport and morphological change would not only represent a fundamental property of braiding dynamics, but has practical applications in numerical modelling, estimating bedload transport rates and, in combination with recent results that show the same threshold is linked to the mobilization of coarse bed material, assessing bed

557 stability (Peirce, 2017). For example, a reach-scaled morphodynamic threshold will likely be easier to characterize in the field than a local grain-scale entrainment threshold, which is difficult to define due to the complex interactions between local shear stress, grain size, and bed structure (Buffington and Montgomery, 1997; Yager and Schott, 2013), especially in large, complex braided rivers. Therefore, general morphodynamic thresholds have the potential to simplify data collection in the field as well as numerical model input parameters, which currently rely on detailed grain size information and entrainment thresholds (Ashmore et al., 2011). In addition, in braided rivers where ecological functioning is paramount, a general threshold for bedload transport and morphological change could help define the disturbance regimes and spatial extent of the bed necessary for habitat restoration and management (Piegay et al., 2006; Bertoldi et al., 2010).

Aside from the above findings, this research highlights the value and importance of morphological methods and physical modelling for understanding and estimating channel evolution and bedload transport rates in dynamic rivers linking braiding rivers (Ashmore and Church, 1998; Williams et al., 2016b). To date, field data on braided river channel topography is limited by low spatial and temporal frequency and a lack of simultaneous bedload transport rates (Bertoldi et al., 2010; Church and Ferguson, 2015; Williams et al., 2016b; Vericat et al., 2017). Here, the use of a physical model allowed for the collection of high-resolution, spatially distributed data of braided river processes and bedload transport rates that contribute to our understanding of the fundamentals of braided river morphodynamics. These data and corresponding analysis can inform, assess, and assist in developing numerical models of braiding morphodynamics and

bedload flux (Bertoldi et al., 2009a; Williams, 2012; Church and Ferguson, 2015; Lugo et al., 2015), which require calibration and validation with high-resolution 3-dimensional surveys of braided rivers (Williams et al., 2016a; Redolfi et al., 2017).

Also, while the research here focused on braided river morphologies, Lugo et al., (2015) used lateral confinement experiments in uniform sand to show that a general relationship between active width (in that case, instantaneous), and dimensionless stream power may not be restricted to braiding rivers, but seems to apply to transitioning (i.e., wandering) as well. Additional experiments should look at these relationships across a greater variety of river morphologies to see if morphodynamic thresholds like those found here are unique to multi-threaded rivers. If so, they could represent a new avenue for defining the transition between meandering and braiding rivers, a useful tool for river channel design, restoration, and characterization (Kleinhans and van den Berg, 2011). Finally, in light of advancements in high-resolution topography methods (Vericat et al., 2017), it may be possible in the future to gather larger datasets of active width, wetted width, and ABI, tied to known discharge conditions, in natural rivers, which can be used to further verify and scale our results.

Overall, we propose that future research in complex gravel-bed rivers consider investigating channel-scale morphodynamic thresholds, which might be more meaningful, and more efficient, in terms of understanding overall channel change and bedload transport rates than thresholds strictly focused on grain-scale dynamics. From here, the ability to better model and predict dynamic channel evolution and bedload transport rates in braided rivers has implications for informing river management decisions like those related to the assessment of flood risk, protection of infrastructure,

and the restoration and preservation of ecological functioning (Marti and Bezzola, 2006; Piegay et al., 2006; Williams et al., 2016b).

Conclusions

Using the largest dataset of its kind, this research highlights that the morphological active width is an important attribute of braided river morphodynamics and that, while spatially and temporally variable, it has a very strong positive and linear relationship with total stream power, bulk change, and active braiding intensity.

Additionally, bedload transport rates and the morphological active width correlate across a range of stream power and have similar lower thresholds of detection, allowing us to conclude that bedload transport is strongly driven by morphological change in these rivers, which is well characterized by active width. Furthermore, during these experiments the morphological active depth was much less sensitive to changes in total stream power and discharge than the morphological active width, indicating that the active width is more important in terms of characterizing morphological change and predicting bedload flux in braiding rivers.

All measures of morphological channel change (i.e., active width, active depth, and bulk change) as well as bedload transport rates, were largely undetectable below the same lower total stream power threshold of 0.17 W m^{-1} or a dimensionless stream power of 0.09, indicating that the bedload entrainment threshold is the same as the threshold for measurable morphological change and active braiding. This defines a morphological threshold for bedload transport and supports the use of reach-scale morphodynamics, in which morphological active width is a central variable, rather than classical grain-

scale hydraulics for analyzing bedload transport in braiding rivers. We propose that future research investigate additional reach-scale morphodynamic feedback systems rather than strictly grain-scale hydraulically-based models of bedload transport, especially in morphologically-driven braided river systems.

Acknowledgements

This research was supported by a Natural Sciences and Engineering Research Council Discovery Grant (41186-2012) to P. Ashmore. Flume construction was supported by the Canada Foundation for Innovation and Newalta Resources Inc. Additional support was provided by the Vanier Canada Graduate Scholarship awarded to S. Peirce. Thank you to everyone who assisted with the experiments, including Lara Middleton and Danielle Barr. Thank you to Karen VanKerkoerle for assisting with the graphics.

References

Ashmore P. 1988. Bed load transport in braided gravel-bed stream models. Earth Surface Processes and Landforms **13**: 677–695.DOI: 10.1002/esp.3290130803

Ashmore P. 1991a. Channel Morphology and Bed Load Pulses in Braided, Gravel-Bed Streams. Geografiska Annaler. Series A, Physical Geography **73**: 37.DOI: 10.2307/521212

Ashmore P. 1991b. How do gravel-bed rivers braid? Canadian Journal of Earth Sciences **28**: 326–341.DOI: 10.1139/e91-030

Ashmore P. 2007. Laboratory modelling of gravel braided stream morphology. Earth Surface Processes and Landforms **7**: 201–225.DOI: 10.1002/esp.3290070301

Ashmore P, Bertoldi W, Tobias Gardner J, Gardner JT. 2011. Active width of gravel-bed braided rivers. Earth Surface Processes and Landforms **36**: 1510–1521.DOI: 10.1002/esp.2182

Ashmore P, Church M. 1998. Sediment transport and river morphology: a paradigm for study. In Gravel-Bed Rivers in the Environment , . 115–148.

Ashmore P, Parker G. 1983. Confluence scour in coarse braided streams. Water Resources Research **19**: 392–402.DOI: 10.1029/WR019i002p00392

Ashmore P, Sauks E. 2006. Prediction of discharge from water surface width in a braided river with implications for at-a-station hydraulic geometry. Water Resources Research **42**: 1–11.DOI: 10.1029/2005WR003993

Bertoldi W, Ashmore P, Tubino M. 2009a. A method for estimating the mean bed load flux in braided rivers. Geomorphology **103**: 330–340.DOI: 10.1016/j.geomorph.2008.06.014

Bertoldi W, Zanoni L, Tubino M. 2009b. Planform dynamics of braided streams. Earth Surface Processes and Landforms **34**: 547–557.DOI: 10.1002/esp

Bertoldi W, Zanoni L, Tubino M. 2010. Assessment of morphological changes induced by flow and flood pulses in a gravel bed braided river: The Tagliamento River (Italy). Geomorphology **114**: 348–360.DOI: 10.1016/j.geomorph.2009.07.017

Buffington JM, Montgomery DR. 1997. A systematic analysis of eight decades of incipient motion studies, with special reference to gravel-bedded rivers. Water Resources Research **33**: 1993–2029.DOI: 10.1029/96WR03190

667 Carson MA, Griffiths GA. 1989. Gravel transport in the braided Waimakariri River:
668 Mechanisms, measurements and predictions. Journal of Hydrology **109**: 201–220.DOI:
669 10.1016/0022-1694(89)90016-4

670 Church M, Ferguson RI. 2015. Morphodynamics: Rivers beyond steady state. Water
671 Resources Research **51**: 1883–1897.DOI: 10.1002/2014WR016862

672 Davies T. 1987. Problems of bed load transport in braided gravel-bed rivers. In
673 Sediment Transfer in Gravel-Bed Rivers , Thorne CR, Bathurst JC, and Hey RD (eds).
674 John Wiley & Sons; 793–811.

675 Davoren A, Mosley MP. 1986. Observations of bedload movement, bar development
676 and sediment supply in the braided Ohau river. Earth Surface Processes and
677 Landforms **11**: 643–652.DOI: 10.1002/esp.3290110607

678 Dietrich WE, Kirchner JW, Ikeda H, Iseya F. 1989. Sediment supply and the
679 development of the coarse surface layer in gravel-bedded rivers. Nature **340**: 215–
680 217.DOI: 10.1038/340215a0

681 Egozi R, Ashmore P. 2008. Defining and measuring braiding intensity. Earth Surface
682 Processes and Landforms **33**: 2121–2138.DOI: 10.1002/esp.1658

683 Egozi R, Ashmore P. 2009. Experimental analysis of braided channel pattern response
684 to increased discharge. Journal of Geophysical Research **114**: F02012.DOI:
685 10.1029/2008JF001099

686 Ferguson RII. 2003. The missing dimension: Effects of lateral variation on 1-D
687 calculations of fluvial bedload transport. Geomorphology **56**: 1–14.DOI: 10.1016/S0169-

555X(03)00042-4

Haschenburger JK, Church M. 1998. Bed material transport estimated from the virtual velocity of sediment. Earth Surface Processes and Landforms **23**: 791–808.DOI: 10.1002/(SICI)1096-9837(199809)23:9<791::AID-ESP888>3.0.CO;2-X

Haschenburger JK, Wilcock PR. 2003. Partial transport in a natural gravel bed channel. Water Resources Research **39**: 1–9.DOI: 10.1029/2002WR001532

Hoey TB, Sutherland AJ. 1991. Channel morphology and bedload pulses in braided rivers: a laboratory study. Earth Surface Processes and Landforms **16**: 447–462.DOI: 10.1002/esp.3290160506

Kasprak A, Wheaton JM, Ashmore P, Hensleigh JW, Peirce S. 2015. The relationship between particle travel distance and channel morphology: Results from physical models of braided rivers. Journal of Geophysical Research: Earth Surface **120**: 55–74.DOI: 10.1002/2014JF003310

Kleinhans MG, van den Berg JH. 2011. River channel and bar patterns explained and predicted by an empirical and a physics-based method. Earth Surface Processes and Landforms **36**: 721–738.DOI: 10.1002/esp.2090

Lindsay JB, Ashmore P. 2002. The effects of survey frequency on estimates of scour and fill in a braided river model. Earth Surface Processes and Landforms **27**: 27–43.DOI: 10.1002/esp.282

Lisle TE, Nelson JM, Pitlick J, Madej MA, Barkett BL. 2000. Variability of bed mobility in natural, gravel-bed channels and adjustments to sediment load at local and reach

scales. Water Resources Research **36**: 3743–3755.DOI: 10.1029/2000WR900238

Lugo GAG, Bertoldi W, Henshaw AJ, Gurnell AM. 2015. The effect of lateral confinement on gravel bed river morphology. Water Resources Research **51**: 7145–7158.DOI: 10.1002/2015WR017081

Marti C, Bezzola GR. 2006. Bed Load Transport in Braided Gravel-Bed Rivers. In Braided Rivers: Process, Deposits, Ecology and Management , . Blackwell Publishing Ltd.: Oxford, UK; 199–215.

Morgan JA, Brogan DJ, Nelson PA. 2016. Application of Structure-from-Motion photogrammetry in laboratory flumes. Geomorphology **276**: 125–143.DOI: 10.1016/j.geomorph.2016.10.021

Mosley MP. 1983. Response of braided rivers to changing discharge. Journal of Hydrology New Zealand **22**: 18–67.

Mosley MP. 1987. Re: Field Measurements in a Gravel-bed River which Confirm the Theory of White et al. In Sediment Transport in Gravel-Bed Rivers , . John Wiley & Sons Ltd.; 506–508.

Mosley MPP. 1982. Analysis of the Effect of Changing Discharge on Channel Morphology and Instream Uses in a Braided River, Ohau River, New Zealand. Water Resources Research **18**: 800–812.DOI: 10.1029/WR018i004p00800

Peakall J, Ashworth PJ, Best JJLJJL. 1996. Physical Modelling in Fluvial Geomorphology : Principles , Applications and Unresolved Issues. 221–253 pp.

Peirce SEK. 2017. Morphological Bedload Transport in Gravel-Bed Braided Rivers, The

University of Western Ontario

Piegay H, Grant G, Nakamura F, Trustrum N. 2006. Braided River Management: from Assessment of River Behaviour to Improved Sustainable Development. In Braided Rivers: Process, Deposits, Ecology and Management , . Blackwell Publishing Ltd.: Oxford, UK; 257–275.

Recking A, Piton G, Vazquez-Tarrio D, Parker G. 2016. Quantifying the Morphological Print of Bedload Transport. Earth Surface Processes and Landforms **41**: 809–822.DOI: 10.1002/esp.3869

Redolfi M, Guidorizzi L, Tubino M, Bertoldi W. 2017. Capturing the spatiotemporal variability of bedload transport: A time-lapse imagery technique. Earth Surface Processes and Landforms **42**: 1140–1147.DOI: 10.1002/esp.4126

Redolfi M, Tubino M, Bertoldi W, Brasington J. 2016. Analysis of reach-scale elevation distribution in braided rivers: Definition of a new morphologic indicator and estimation of mean quantities. Water Resources Research **52**: 5951–5970.DOI: 10.1002/2015WR017918

Shvidchenko AB, Kopaliani ZD. 1998. Hydraulic Modeling of Bed Load Transport in Gravel-Bed Laba River. Journal of Hydraulic Engineering **124**: 778–785.DOI: 10.1061/(ASCE)0733-9429(1998)124:8(778)

Southard JB, Smith ND, Kuhnle RA. 1984. Chutes and lobes: newly identified elements of braiding in shallow gravelly streams. In Sedimentology of Gravels and Conglomerates , Koster EH and Steel RJ (eds). Canadian Society of Petroleum Geologists; 51–59.

Vericat D, Wheaton JM, Brasington J. 2017. Revisiting the Morphological Approach. In Gravel-Bed Rivers , . John Wiley & Sons, Ltd: Chichester, UK; 121–158.

Warburton J, Davies T. 1994. Variability of bedload transport and channel morphology in a braided river hydraulic model. Earth Surface Processes and Landforms **19**: 403–421.DOI: 10.1002/esp.3290190503

Wheaton JM, Brasington J, Darby SE, Kasprak A, Sear DA, Vericat D. 2013. Morphodynamic signatures of braiding mechanisms as expressed through change in sediment storage in a gravel-bed river. Journal of Geophysical Research: Earth Surface **118**: 759–779.DOI: 10.1002/jgrf.20060

Williams RD. 2012. DEMs of Difference. Geomorphological Techniques **2**: 1–17.DOI: 2047-0371

Williams RD, Brasington J, Hicks DM. 2016a. Numerical Modelling of Braided River Morphodynamics: Review and Future Challenges. Geography Compass **10**: 102–127.DOI: 10.1111/gec3.12260

Williams RD, Measures R, Hicks DM, Brasington J. 2016b. Assessment of a numerical model to reproduce event-scale erosion and deposition distributions in a braided river. Water Resources Research **52**: 6621–6642.DOI: 10.1002/2015WR018491

Williams RD, Rennie CD, Brasington J, Hicks DM, Vericat DD. 2015. Linking the spatial distribution of bed load transport to morphological change during high-flow events in a shallow braided river. Journal of Geophysical Research: Earth Surface **120**: 604–622.DOI: 10.1002/2014JF003346

Yager EM, Schott HE. 2013. The Initiation of Sediment Motion and Formation of Armor Layers. In Treatise on Geomorphology , Shroder JF (ed). Elsevier: San Diego; 87–102.

Young WJ, Davies TRH. 1990. Prediction of bedload transport rates in braided rivers: a hydraulic model study. Journal of Hydrology (NZ) **29**: 75–92.

Young WJ, Warburton J. 1996. Principles and practice of hydraulic modelling of braided gravel-bed rivers. Journal of Hydrology New Zealand **35**: 175–198.DOI: 10.1016/S0301-9322(97)80098-5

Table 1 - Experimental conditions where the experiment number refers to the order in which the experiments were completed, S is % slope of the flume, the discharge (Q) is the estimated discharge (± 5 %) and Ω is total stream power. The experiments were divided into periods of evolution and experimental runs. Runs were divided into two 8 hour blocks, separated by a shorter second round of evolution. The DEM count refers to the number of DEMs used in the reported analysis. Total time is the length of time from the initial straight channel to the end of the final experimental run.

	INITIAL CONDITIONS			*EVOLUTION*		*RUNS*		
EXPERIMENT	SLOPE	DISCHARGE	STREAM POWER					
	S	**Q**	**Ω**	**Initial**	**Second Round**	**Time**	**DEM Count**	**Total Time**
	%	$l\ s^{-1}$	$W\ m^{-1}$	h	h	h		h
1	1.5	0.70	0.10	16	8	16.9	29	40.9
4	1.5	1.65	0.24	42	9	17.0	66	68.0
9	1.5	2.10	0.31	28.25	8	18.25	68	54.5
12	1.5	2.50	0.37	20	2	16.5	65	38.5
13	2	2.10	0.41	12	0.75	16.5	67	29.25
11	1.5	0.7 - 2.1	0.10 - 0.31	24	-	30.25	110	54.25
Totals						115.4	405	285.4

Table 2 - Vertical error estimates for each experiment based on 1 and 3 standard deviation (σ) of the distribution of the elevations for the area of the DEMs that did not undergo morphologic change.

EXPERIMENT	*σ (mm)*	*3σ (mm)*
1	2.4	7.2
4	1.3	3.9
9	1.7	5.1
12	0.96	2.88
13	0.79	2.37
11	1.15	3.45

Table 3 - Summary statistics for average morphological active width as a percent of average wetted width, where n is the number of observations, min and max are the minimum and maximum values, mean is the average, and σ is the standard deviation.

	% ACTIVE WIDTH					
EXPERIMENT	n	Min	Max	Median	Mean	σ
1	4	4.18	9.45	6.49	6.65	2.34
4	8	7.44	27.3	15.9	16.5	7.31
9	8	7.60	17.1	10.6	11.6	3.12
12	8	23.5	31.2	27.6	27.5	2.44
13	8	35.8	58.5	44.1	45.3	7.49
11	26	1.10	28.9	11	11.4	8.94

Table 4 - Summary statistics for bulk change (m^3) for the constant discharge experiments, where min and max are the minimum and maximum values, mean is the average value, and σ is the standard deviation.

	BULK CHANGE (m^3)			
EXPERIMENT	**Minimum**	**Maximum**	**Mean**	**σ**
1	0.0000	0.0026	0.0006	0.0005
4	0.0024	0.0265	0.0106	0.0056
9	0.0061	0.0318	0.0152	0.0059
12	0.0232	0.0642	0.0355	0.0081
13	0.0343	0.0585	0.0470	0.0058

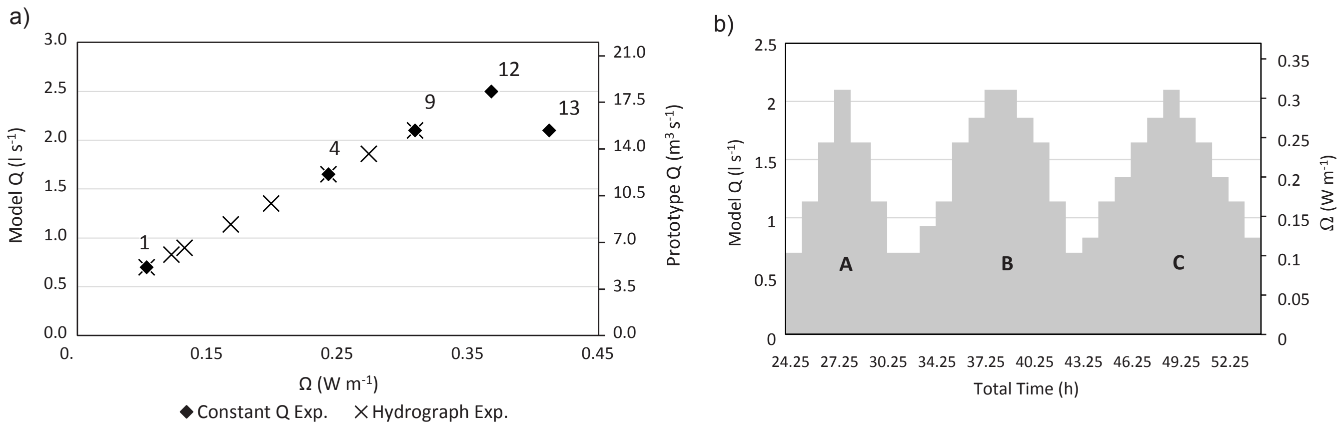

Figure 1 - a) Model discharge (Q) and approximate prototype discharge based on 1:35 length scaling as a function of the model total stream power (Ω) for both the constant discharge and hydrograph experiments. b) Discharge and total stream power of the model for the hydrograph experiments (A, B, and C) as a function of total time.

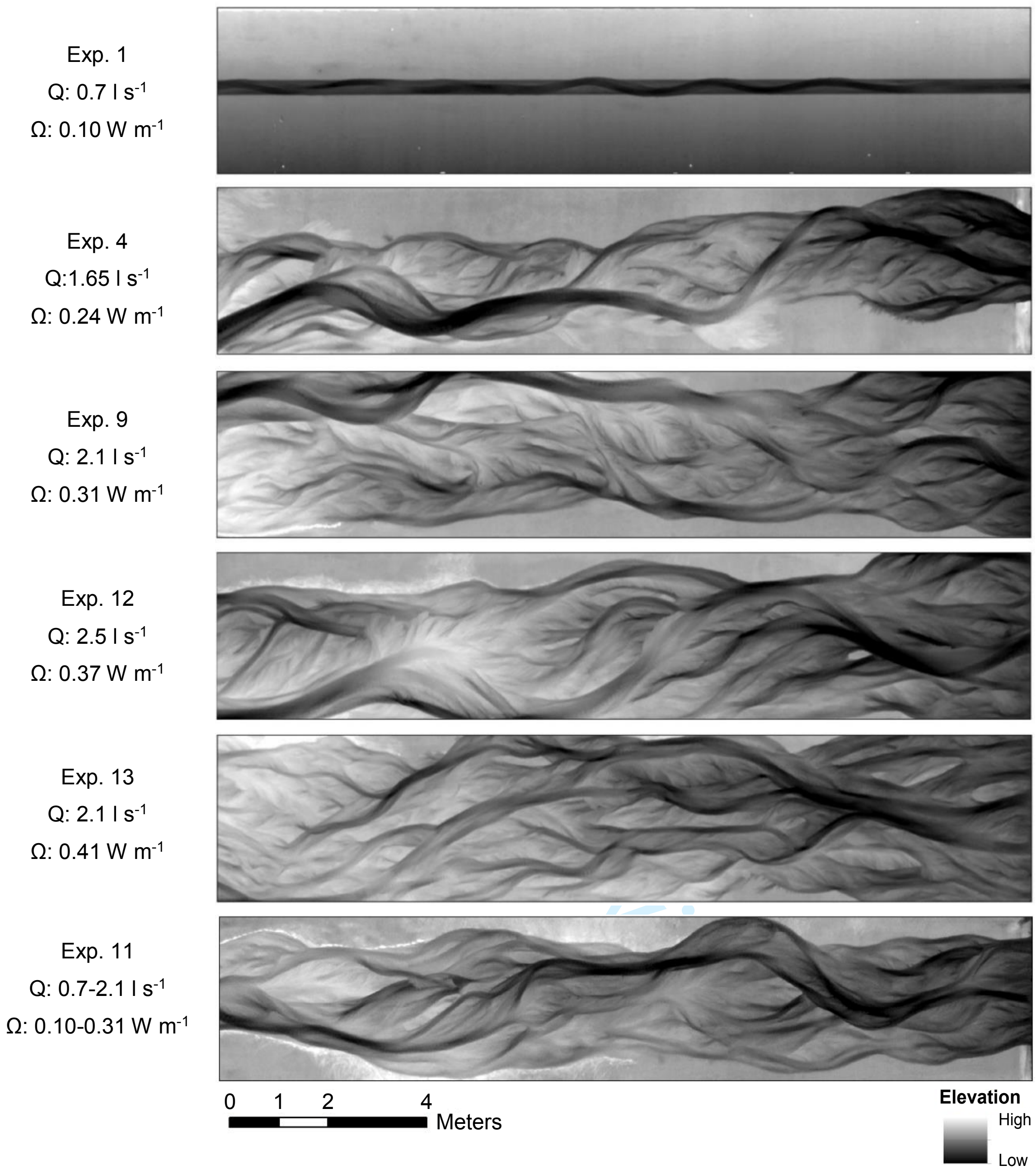

Figure 2 - The final digital elevation models of each experiment, where Q is discharge and Ω is total stream power. Flow was from left to right.

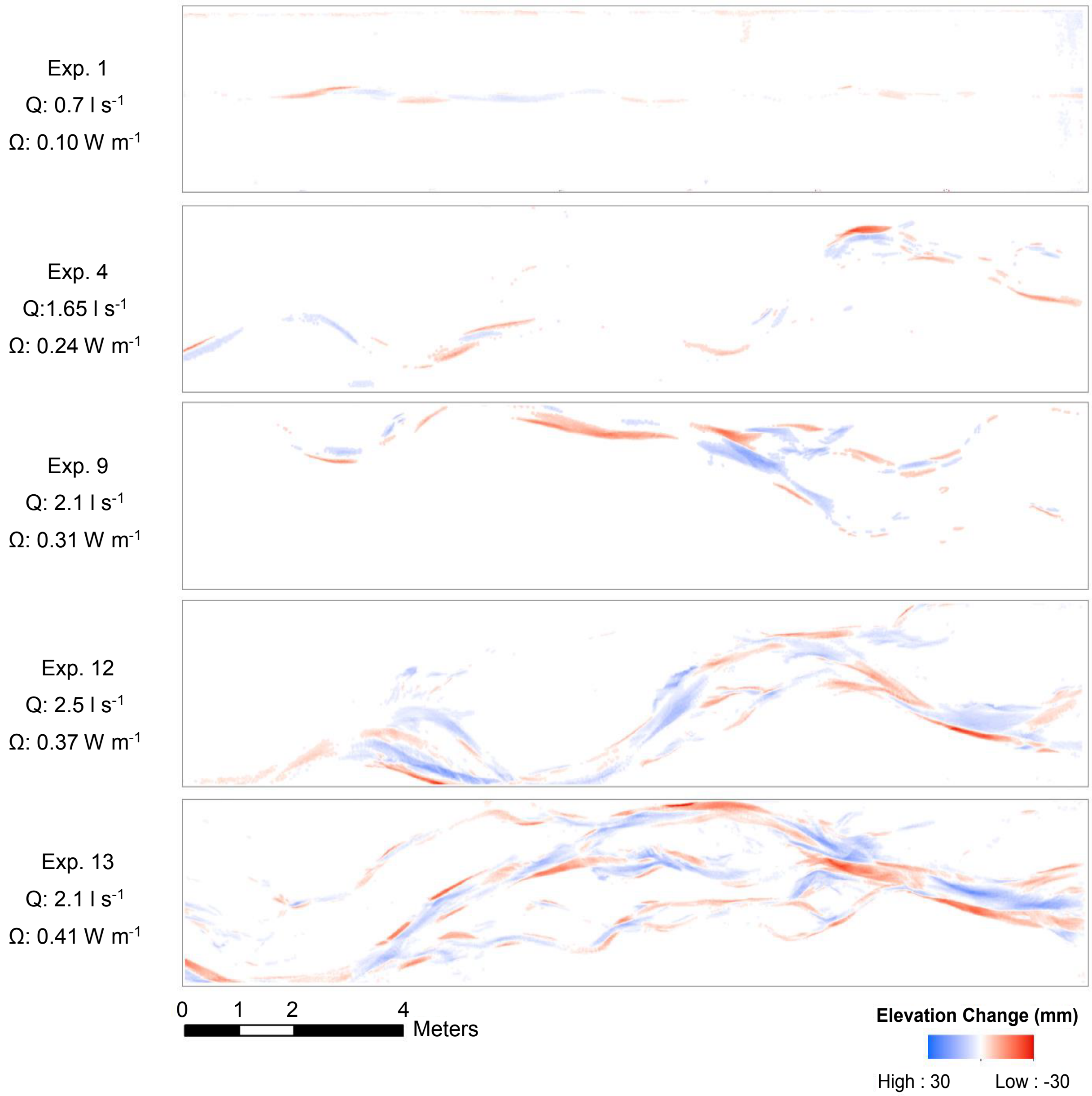

Figure 3 – DEMs of difference generated using the final 2 DEMs from the five constant discharge experiments, where Q is discharge and Ω is total stream power. Flow was from left to right.

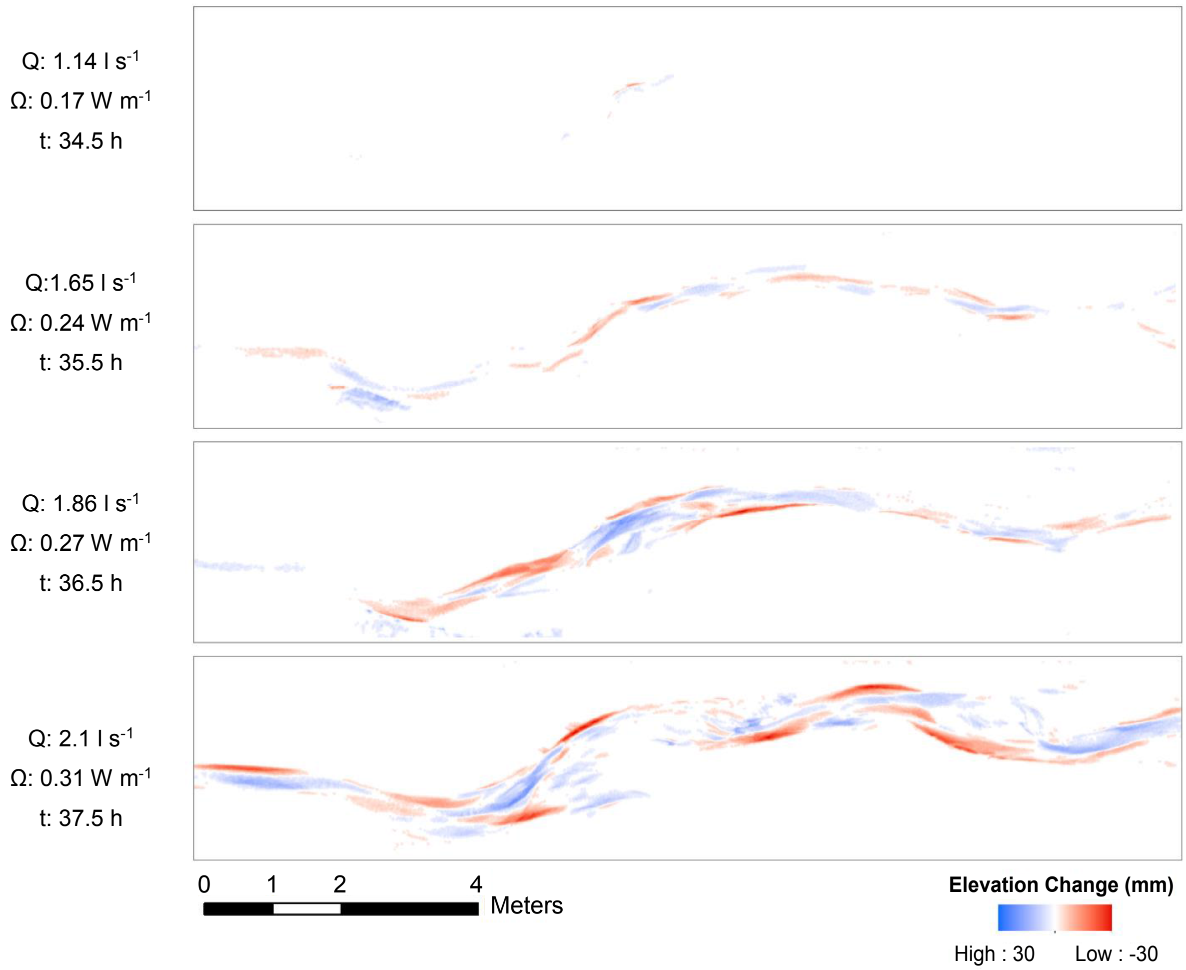

Figure 4 – Example DEMs of difference from the rising limb of hydrograph B, experiment 11, where Q is discharge and Ω is total stream power, and t refers to total time. Flow is from left to right.

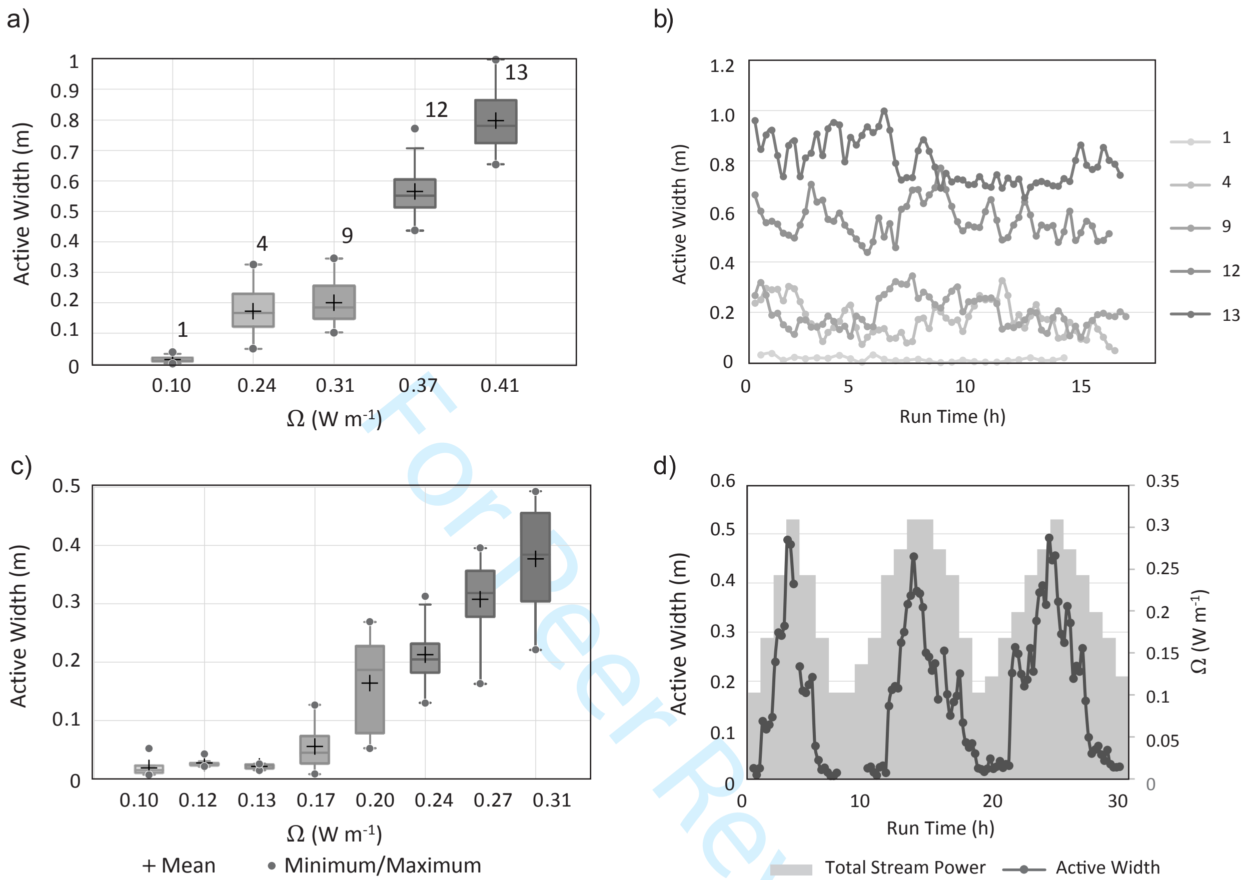

Figure 5 - Reach-averaged morphological active width as a function of total stream power (Ω) and experimental run time for the constant discharge experiments (a and b) and the hydrograph experiments (c and d).

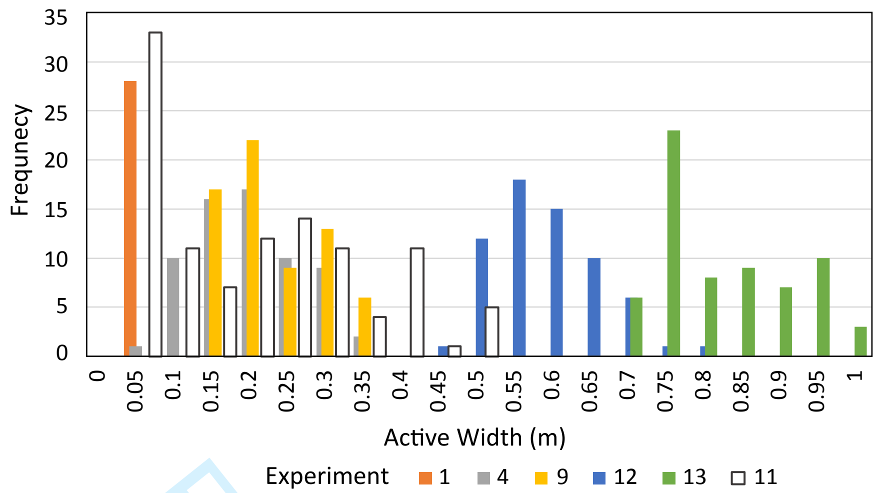

Figure 6 - Frequency distributions of the morphological active widths for all the constant discharge (1, 4, 9, 12 and 13) and hydrograph (11) experiments.

"

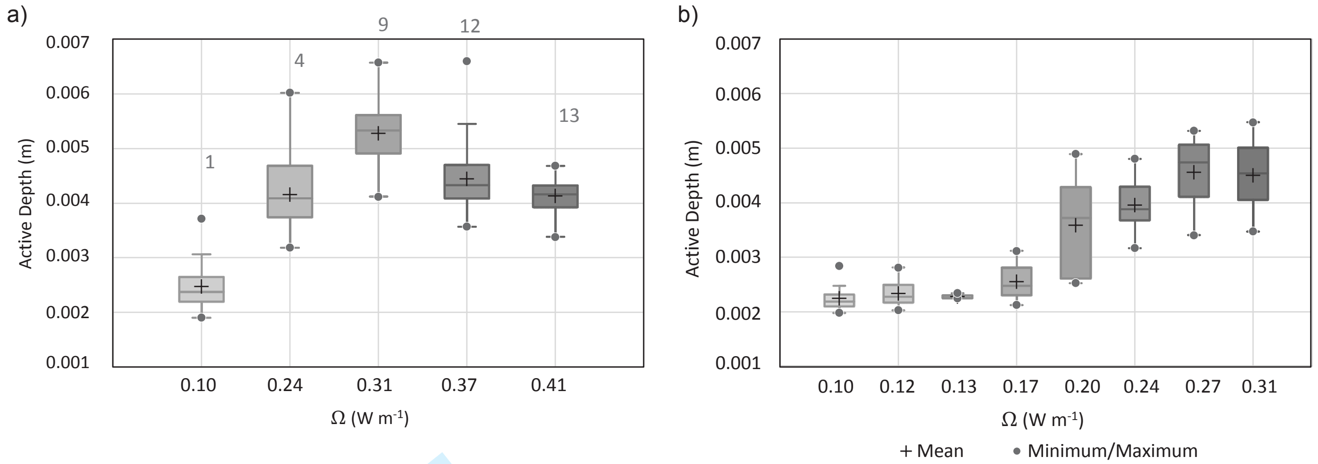

Figure 7 – Reach-averaged morphological active depths versus total stream power (Ω) for the a) constant discharge (1, 4, 9, 12, and 13) and b) hydrograph experiments.

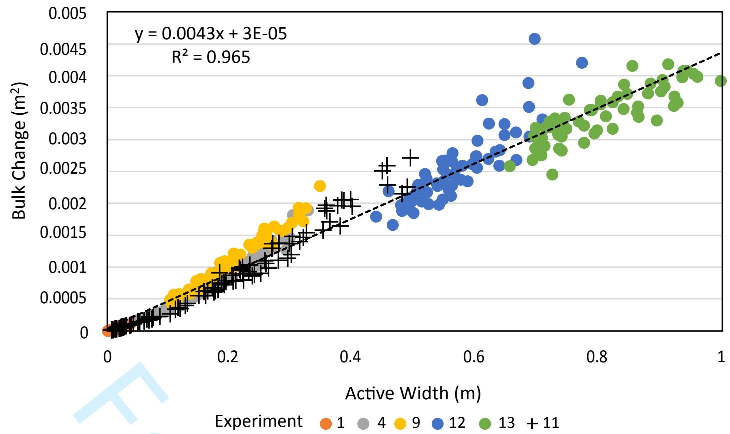

Figure 8 – Reach-averaged bulk change as a function of the reach-averaged morphological active with for the constant discharge (1, 4, 9, 12, and 13) and hydrograph (11) experiments. The dashed line represents the linear regression through all observations.

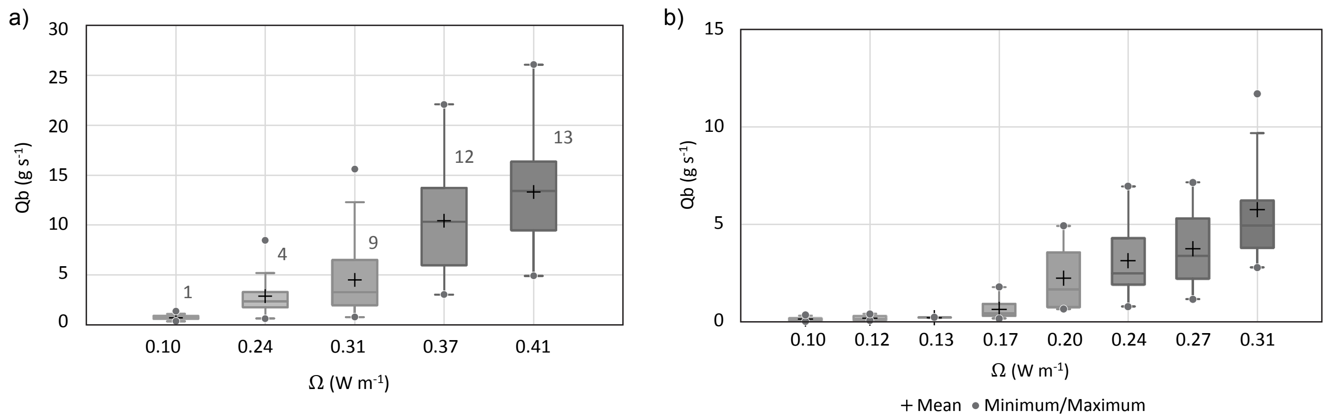

Figure 9 - Bedload transport rates (Qb) for each total stream power (Ω) of the a) constant discharge (1, 4, 9, 12, and 13) and b) hydrograph experiments. Note differences in axes.

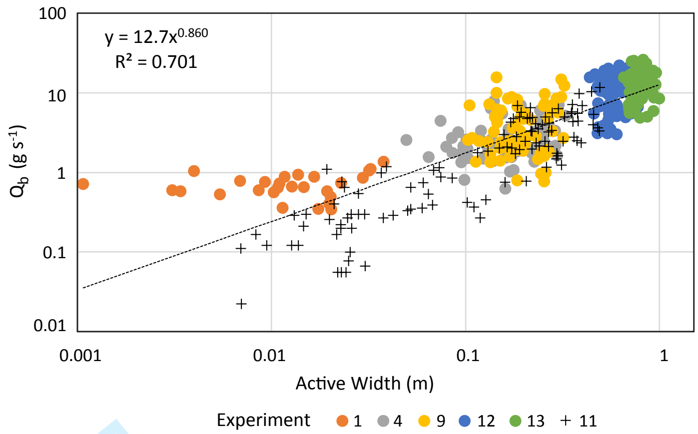

Figure 10 - Bedload transport rate plotted against reach-averaged morphological active width for constant discharge (1, 4, 9, 12 and 13) and hydrograph (11) experiments. The dashed line represents the power regression through all observations.

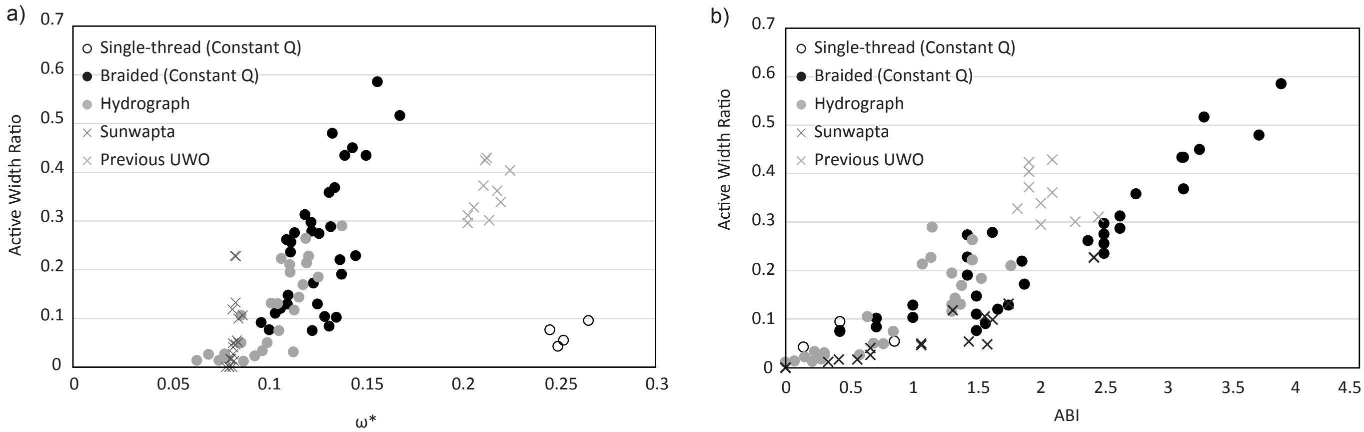

Figure 11 – Reach-averaged morphological active width ratios plotted as a function of a) dimensionless stream power (ω*) and b) active braiding intensity (ABI) combined with field (Sunwapta) and flume (Previous UWO) results from Ashmore et al. (2011), where Q is discharge.

Graphical Information

The Variability in the Morphological Active Width: Results from Physical Models of Gravel-Bed Rivers

Sarah Peirce[1*], Peter Ashmore[1], Pauline Leduc[1]

[1] The University of Western Ontario, London, Ontario, Canada

Key Points

- The morphological active width is a fundamental parameter of braided rivers that increases with total and dimensionless stream power.
- The morphological active width has a positive relationship with bulk change, bedload transport, and active braiding intensity.
- Both morphological change and bedload transport rates were largely undetectable under a dimensionless stream power of ~0.09.